



*Supplement of*

## **Global and regional carbon budget for 2015–2020 inferred from OCO-2 based on an ensemble Kalman filter coupled with GEOS-Chem**

**Yawen Kong et al.**

*Correspondence to:* Bo Zheng (bozheng@sz.tsinghua.edu.cn)

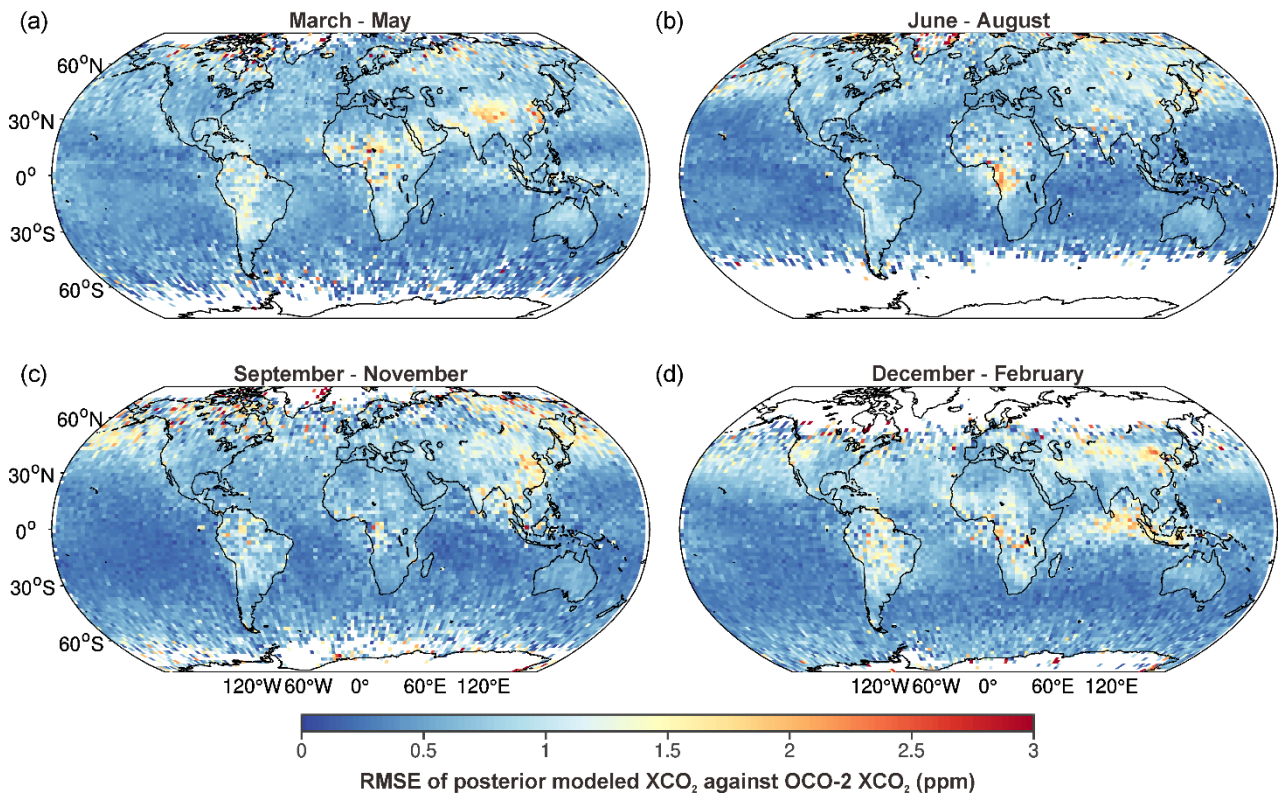
The copyright of individual parts of the supplement might differ from the article licence.

**Table S1. Surface flask measurement stations used for inversion model evaluation.**

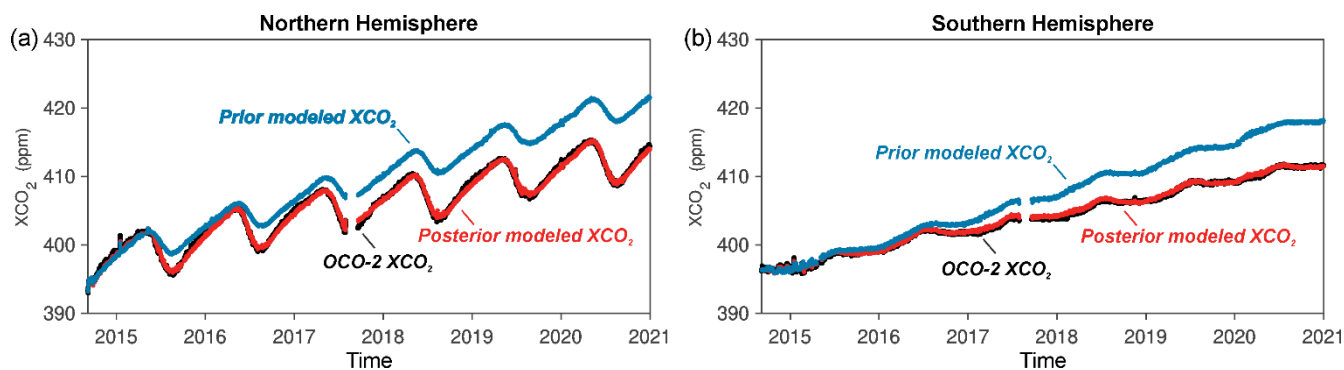
Station code	Latitude	Longitude	Elevation (m a.s.l.)	Station code	Latitude	Longitude	Elevation (m a.s.l.)
ALT	82.45	-62.51	190	IZO	28.31	-16.50	2377.9
ZEP	78.91	11.89	479	MID	28.21	-177.38	16
TIK	71.60	128.89	29	KEY	25.67	-80.16	6
BRW	71.32	-156.61	27.5	LLN	23.47	120.87	2867
PSL	67.97	24.12	570	ASK	23.26	5.63	2715
ICE	63.40	-20.29	127	DSI	20.70	116.73	8
CBA	55.21	-162.72	57.04	KUM	19.52	-154.82	8
MHD	53.33	-9.90	26	GMI	13.39	144.66	5
SHM	52.71	174.13	28	RPB	13.16	-59.43	20
TAC	52.52	1.14	236	CHR	1.70	-157.15	5
OXK	50.03	11.81	1172	BKT	-0.20	100.32	875
HPB	47.80	11.02	941	SEY	-4.68	55.53	7
HUN	46.95	16.65	344	NAT	-5.51	-35.26	20
UUM	44.45	111.10	1012	ASC	-7.97	-14.40	90
CIB	41.81	-4.93	850	SMO	-14.25	-170.56	47
THD	41.05	-124.15	112	NMB	-23.58	15.03	461
HSU	41.03	-124.57	7.6	EIC	-27.16	-109.43	69
SDZ	40.65	117.12	298	CPT	-34.35	18.49	260
UTA	39.90	-113.72	1332	CGO	-40.68	144.69	164
AZR	38.77	-27.38	24	BHD	-41.41	174.87	90
TAP	36.74	126.13	21	CRZ	-46.43	51.85	202
SGP	36.61	-97.49	374	USH	-54.85	-68.31	32
AMY	36.54	126.33	87	PSA	-64.92	-64.00	15
LMP	35.52	12.62	50	SYO	-69.01	39.59	19
BMW	32.26	-64.88	60	HBA	-75.61	-26.21	35
WIS	30.86	34.78	482	SPO	-89.98	-24.80	2815

15 **Table S2. Aircraft measurement programs used for inversion model evaluation.**

Measurement program code	Measurement program name	DOI	Reference
ABOVE	Arctic-Boreal Vulnerability Experiment	10.3334/ORNLDAAC/1658	Sweeney and McKain (2019)
ACT	Atmospheric Carbon and Transport-America	10.3334/ORNLDAAC/1593	Davis et al. (2018)
TOM	ATom, Atmospheric Tomography Mission	10.3334/ORNLDAAC/1732	McKain and Sweeney (2021)



20 **Figure S1: Spatial and seasonal distributions of RMSE for the modeled XCO<sub>2</sub> against the OCO-2 XCO<sub>2</sub> between 2015 and 2020.** The modeled XCO<sub>2</sub> are derived from the GEOS-Chem model simulation driven by the posterior fluxes of our reference inversion. The RMSE is calculated and present for March–May (a), June–August (b), September–November (c), and December–February (d). The values shown here are the annual averages between 2015 and 2020.



25 **Figure S2: Comparisons of the GEOS-Chem modeled  $XCO_2$  with OCO-2  $XCO_2$  at the daily scale between 2015 and 2020.** The GEOS-Chem simulations driven by the prior (blue curves) and the posterior (red curves) fluxes of our reference inversion are evaluated against the OCO-2  $XCO_2$  retrievals (black curves) over the Northern Hemisphere (a) and the Southern Hemisphere (b), respectively.

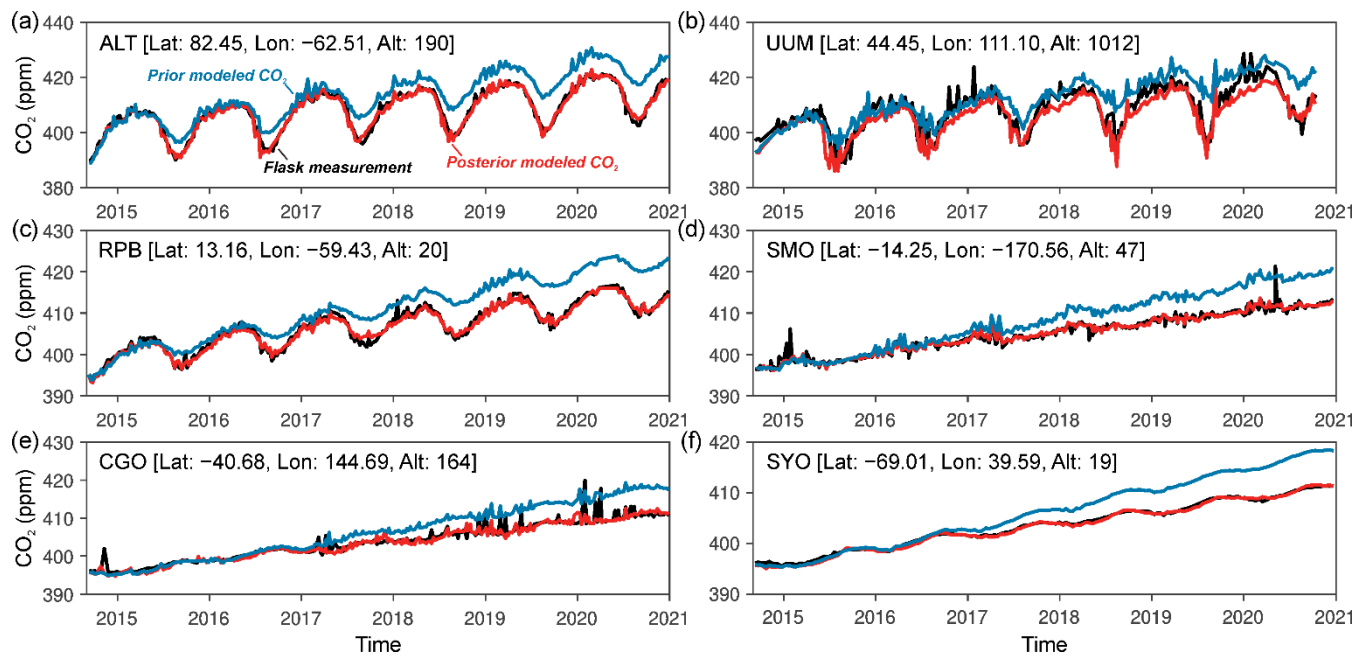


**Figure S3: Comparisons of the GEOS-Chem modeled CO<sub>2</sub> concentrations with surface flask measurement at the daily scale between 2015 and 2020.** The GEOS-Chem simulations driven by the prior (blue curves) and the posterior (red curves) fluxes of our reference inversion are evaluated against the flask measurement (black curves) from the surface stations of ALT (a), UUM (b), RPB (c), SMO (d), CGO (e), and SYO (f), which vary by latitude and by altitude and have continuous measurement records since 2014.

30

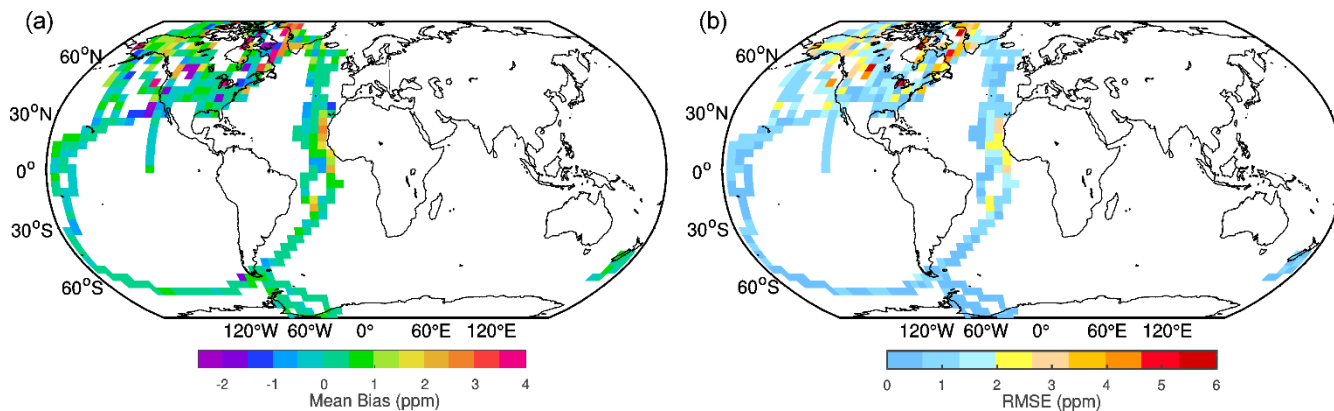
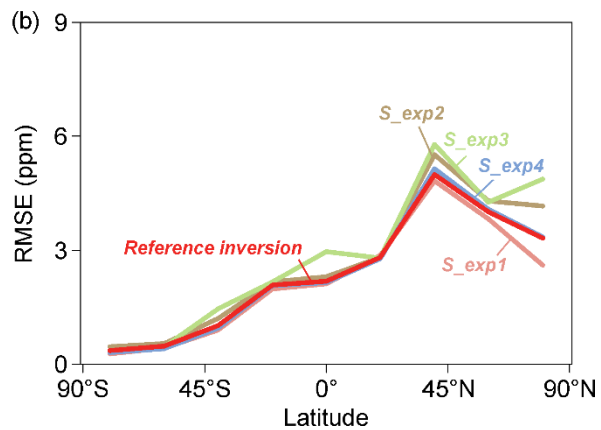
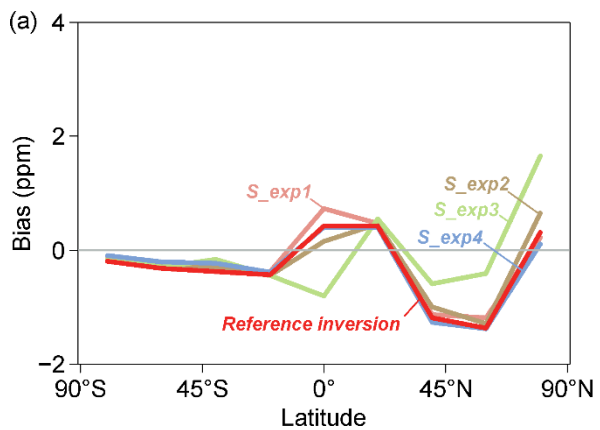


**Figure S4: Mean bias and RMSE for the GEOS-Chem modeled CO<sub>2</sub> concentrations against aircraft measurement.** The GEOS-Chem simulations driven by the posterior fluxes of our reference inversion are evaluated against the aircraft observations above 3000 m with biases (a) and RMSEs (b) shown in the GEOS-Chem 4° × 5° grid cells. The aircraft measurement programs are shown in Table S2.



35

**Figure S5: Comparisons of the GEOS-Chem modeled dry air mole fractions of CO<sub>2</sub> with surface measurements for 2015.** The simulations driven by posterior fluxes from our reference inversion and four sensitivity inversions in 2015 are evaluated against surface flask observations for modeled biases (a) and RMSEs (b). The measurement sites are summarized in Table S1.

## References

- 40 Davis, K. J., Obland, M.D., Lin, B., Lauvaux, T., O'Dell, C., Meadows, B., Browell, E.V., DiGangi, J.P., Sweeney, C., McGill, M. J., Barrick, J.D., Nehrir, A. R., Yang, M. M., Bennett, J. R., Baier, B. C., Roiger, A., Pal, S., Gerken, T., Fried, A., Feng, S., Shrestha, R., Shook, M.A., Chen, G., Campbell, L. J., Barkley, Z. R., and Pauly, R. M.: ACT-America: L3 Merged In Situ Atmospheric Trace Gases and Flask Data, Eastern USA, ORNL DAAC, Oak Ridge, Tennessee, USA, doi: 10.3334/ORNLDAAC/1593, 2018.
- 45 McKain, K., and Sweeney, C.: ATom: CO<sub>2</sub>, CH<sub>4</sub>, and CO Measurements from Picarro, 2016-2018. ORNL DAAC, Oak Ridge, Tennessee, USA, doi: 10.3334/ORNLDAAC/1732, 2021.
- Sweeney, C., and McKain, K.: ABoVE: Atmospheric Profiles of CO, CO<sub>2</sub> and CH<sub>4</sub> Concentrations from Arctic-CAP, 2017, ORNL DAAC, Oak Ridge, Tennessee, USA, doi: 10.3334/ORNLDAAC/1658, 2019.